

Topologically protected frequency control of broadband signals in dynamically modulated waveguide arrays

Francesco S. Piccioli,^{1,2} Alexander Szameit,² and Iacopo Carusotto¹

¹*INO-CNR BEC Center and Dipartimento di Fisica, Università di Trento, 38123 Trento, Italy*

²*Institute for Physics, University of Rostock, Albert-Einstein-Str. 23, 18059 Rostock, Germany**

We theoretically propose a synthetic frequency dimension scheme to control the spectrum of a light beam propagating through an array of evanescently coupled waveguides modulated in time by a propagating sound wave via the acousto-optical effect. Configurations are identified where the emerging two-dimensional synthetic space-frequency lattice displays a non-trivial topological band structure. The corresponding chiral edge states can be exploited to manipulate the frequency spectrum of an incident beam in a robust way. In contrast to previous works, our proposal is not based on discrete high-Q cavity modes, which paves the way to the manipulation of broadband signals.

The control of the frequency spectrum of a light beam is of high importance in a number of photonic applications, from high speed communications to quantum technologies. In telecommunications, the concept of Frequency Division Multiplexing (FDM) is at the basis of 5G technology and allows to increase the data throughput by superposing in time signals with different carrier frequencies [1]. In quantum optics, entanglement and quantum interference processes involving the frequency and/or temporal degrees of freedom are attracting a strong interest [2–4] and requires careful compensation for frequency mismatch between different emitters [5–7].

In all these applications, the ability of manipulating the spectrum of generic signals is a fundamental basic block in the direction of building complex networks. Among the many processes that can be exploited to this purpose, such as nonlinear optical wave-mixing [8–12] or photon energy lifter [13, 14], a most intriguing one is undoubtedly the dynamical modulation in time of the optical properties of a medium. Such mechanism has been recently exploited to realize synthetic dimensions [15–17] in which the frequency degree of freedom plays the role of an extra physical dimension. This leads to an effective description of light propagation in terms of a higher-dimensional wave equation, where different kind of forces can be engineered to control the dynamics in the full high-dimensional space.

Most of the so far proposed synthetic frequency dimension schemes rely on the dynamical modulation of resonating structures like multi-mode cavities [18, 19], where high quality factors are typically needed. Not only does this impose stringent limits on the fabrication quality, but also restricts the signals to be manipulated to quasi-monochromatic light beams or frequency combs with a spacing commensurate to the free spectral range of the resonators. The severity of this restriction is most apparent when contrasted to the typically broadband nature of telecommunication signals and to the inhomogeneous broadening of quantum emitters.

This limitation can be overcome by replacing resonat-

ing configurations with propagating ones such as optical waveguides. Recent works have started exploring the temporal modulation of isolated LiNbO₃ optical waveguides [20–22] using an RF-driven electro-optical effect. However, many interesting phenomena such as topological effects [15, 23–25] requires at least another dimension. Beside using multi-frequency temporal modulations [26], reciprocal space schemes [27–29], or spin-like degrees of freedom [30], a most direct way to increase the dimensionality is to use evanescently Coupled Waveguide Arrays (CWA) [31].

In this Letter, we propose the use of propagating sound waves to dynamically modulate CWA via the acousto-optic effect. This allows to realize a hybrid synthetic space composed by a spatial and a frequency dimension and, thus, observe topological photonics effects of great interest for applications. The use of sound-induced acousto-optical modulation in laser-written amorphous materials rather than the electro-optic effect in patterned crystalline materials eases fabrication and is compatible with the larger inter-waveguide distances imposed by the long wavelength of the sonic waves considered in this work. As a result, one can make use of standard photonic technology to design a suite of efficient schemes for the coherent manipulation of the carrier and/or the linewidth of broadband signals, taking advantage of topological protection.

Dynamical modulation of a single isolated waveguide–

Let us start from an isolated optical waveguide, whose axis is aligned to the z direction. Restricting to its lowest order mode, the waveguide supports propagating states with a continuous frequency spectrum ω and propagation constant $\kappa_l(\omega)$. Let us now include a monochromatic refractive index modulation of angular frequency ω_m traveling through the surrounding bulk material with a wavevector \mathbf{k}_m forming an angle θ with respect to the waveguide axis (see fig. 1a),

$$\Delta n(\mathbf{r}, t) = 2 \delta n \cos(\mathbf{k}_m \cdot \mathbf{r} - \omega_m t) \quad (1)$$

The effect of this monochromatic spatio-temporal modulation is to linearly couple frequency components that

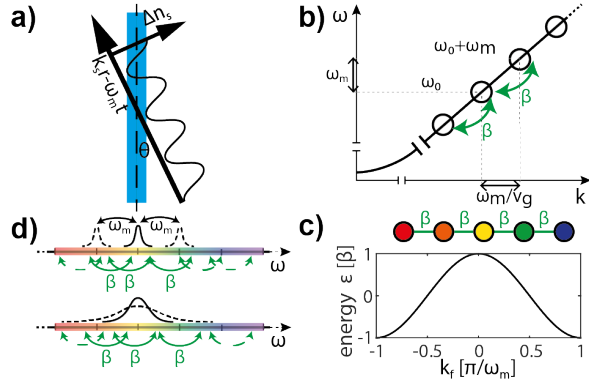


Fig. 1. a) concept of the travelling sound wave used to modulate a single optical waveguide. b) Induced 1D spectral lattice in the dispersion relation of the fundamental waveguide mode. c) Dispersion relation in a modulated waveguide plotted as the light wavevector as a function of the frequency momentum k_f . d) top(bottom) Illustration of the qualitatively different dynamics for narrowband(broadband) light beam compared to the modulation frequency ω_m

are separated by the modulation frequency ω_m (fig.1b). The equation describing the evolution of each frequency component of the light beam then takes the form of a Schrödinger-like equation on a continuous 1D frequency space displaying long range hoppings. Here, the light propagation direction z plays the role of time and the frequency ω plays the role of a space-like variable,

$$i\partial_z E(z, \omega) = \frac{\Delta k}{\omega_m} \omega E(z, \omega) - \beta E(z, \omega \pm \omega_m). \quad (2)$$

In this equation, $\beta = \delta n k_0$ quantifies the hopping amplitude and the phase mismatch $\Delta k = k_m \cos \theta - \omega_m \frac{\partial \kappa_l}{\partial \omega}$ between the modulation and the optical wave provides a diagonal term $\frac{\Delta k}{\omega_m} \omega E(z, \omega)$ representing a (static) scalar potential in the direction of increasing light frequency. The details of the derivation can be found in the Supplemental Material [32].

In the limiting case of a monochromatic light input at ω_0 , the rigorous form (2) of the propagation equation can be rewritten in a more familiar form. In this case, the symmetry of the system allows to restrict our attention to a discrete set of frequencies $\{\omega_n\} = \omega_0 + n\omega_m$. Then, upon the definition of the frequency components $a_n(z) = E(z, \omega_n)$, the evolution (2) can be rewritten [15, 18, 32] in terms of a discrete 1D lattice corresponding to the synthetic dimension associated to the light frequency (fig.1c),

$$i\partial_z a_n(z) = n\Delta k a_n - \beta a_{n\pm 1}. \quad (3)$$

Given the peculiar connectivity induced by the long range hopping that is pictorially depicted in fig.1d, the effectively discrete or continuous character of the synthetic dimension is determined by the bandwidth of the

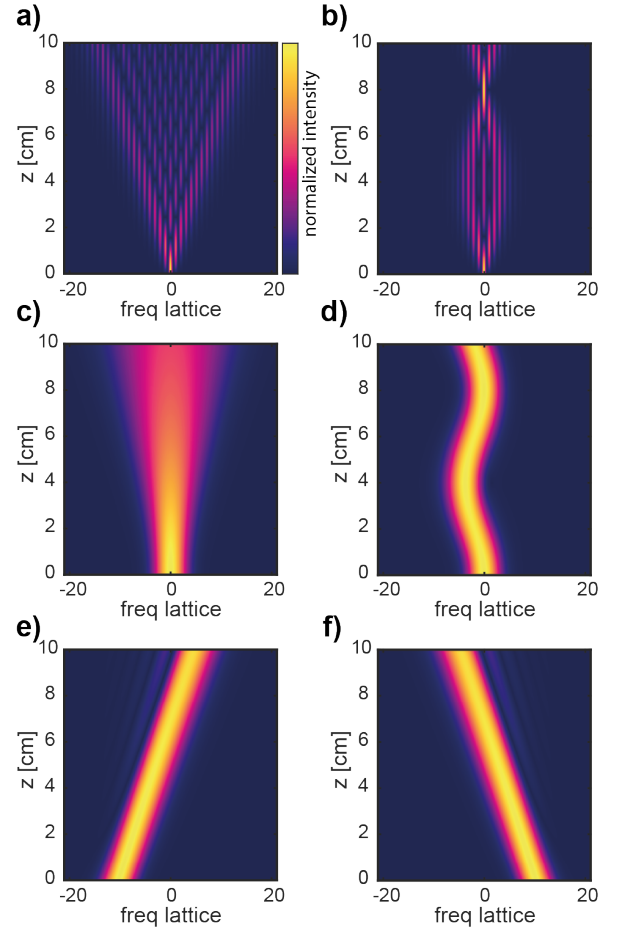


Fig. 2. Power spectral density of light travelling in a dynamically modulated waveguide as a function of the propagation distance. **a,c**) Diffraction in the frequency space of a narrowband (**a**) or broadband(**c**) signal with respectively $\Delta\omega = 0.3\omega_m$ and $\Delta\omega = 3\omega_m$. **b,d**) Bloch oscillations in the frequency space of the same narrowband (**b**) and broadband(**d**) signals in the presence of a finite phase-mismatch $\Delta k = \beta/2$. **e,f**) Propagation in the frequency space of the broadband signal injected in the waveguide, now with a time delay $\Delta T = \pm\pi/(2\omega_m)$. For this and all the following simulations 800 nm light and a $\delta n = 5 \times 10^{-5}$ refractive index modulation are considered

input beam, chosen for simplicity with a Gaussian spectral shape,

$$\psi_0(\omega) = e^{-\left(\frac{\omega-\omega_0}{\Delta\omega}\right)^2} e^{-ik_f(\omega-\omega_0)} \quad (4)$$

If the spectrum of an input signal is limited within the hopping range $\Delta\omega \ll \omega_m$ (namely the pulse duration $\tau = 2\sqrt{2\log 2}/\Delta\omega$ is longer than the modulation period $T_m = 2\pi/\omega_m$), as in the top line of fig.1d, then all the components of such input signal excite a single cell in the synthetic space and the dynamics of the frequency spectrum follows that of a monochromatic beam discussed above[20, 21]. Examples of possible behaviours are shown in fig.2a,b where a narrowband signal with $\Delta\omega = 0.3\omega_m$

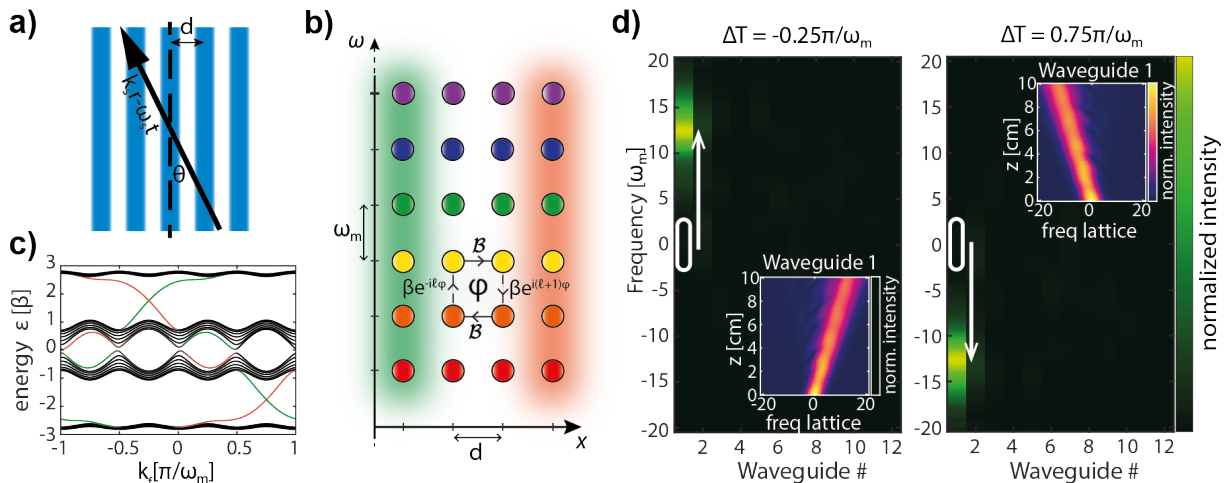


Fig. 3. **a)** Scheme of a dynamically modulated array of coupled waveguides. **b)** scheme of the two-dimensional Harper-Hofstadter lattice in the hybrid space composed by the spatial and the frequency dimensions with the corresponding hopping amplitudes. **c)** Dispersion relation of a $\Phi = 1/4$ HH lattice. Edge states are color-coded accordingly to their localization as in the **b)** panel: green is for left-edge localized states and orange for right-edge. **d)** Topological frequency conversion on the right edge of the modulated waveguide array when up/down-shifting topological modes are selectively excited using properly delayed pulses. Main panels show the intensity distribution in the hybrid frequency-space of output light. The insets display the power spectral density during propagation on the excited waveguide. Same parameters as in Fig.2.

is used as an input: In fig.2a, the envelope of the spectrum gets broadened by the diffraction in the discrete frequency space whereas in fig.2b Bloch oscillations arise as a result of the linear potential induced by a phase mismatch Δk .

An even richer physics is found when the bandwidth of the injected light pulse is increased to $\Delta\omega \gg \omega_m$ (i.e. $\tau \ll T_m$) and encompasses several cells. In this case, the dynamical modulation induces a coupling between different frequencies of the same broadband input signal (fig.1d) and the dynamics resembles the one of continuous space (fig.2c-f). Most importantly, as the input signal excites a wide region of the spectral lattice, the phase relation between the frequency components becomes relevant. This is determined by the value of the *frequency momentum* k_f parameter in equation (4), which plays the same role of the momentum of a quantum particle or the transverse wavevector in real space waveguide arrays [31]. Interestingly, whereas k -space momentum selection in CWAs is typically achieved by tilting the incident beam with respect to the waveguide axis, here the reciprocal space of the frequency dimension is the real time and k_f can be understood as the time-delay (ΔT) of the light pulse with respect to the external modulation. As a consequence, specific *frequency momenta* can be simply excited with an appropriate choice of the incident pulse delay ΔT .

Examples of the evolution of broadband pulses with $\Delta\omega = 3\omega_m$ are displayed in fig.2c-f. In particular, in fig.2c, $\Delta T = 0$ is chosen, which results in a ballistic broadening of the input spectrum in agreement with the dispersion relation plotted in fig.1c. In fig.2(d), a fi-

nite phase mismatch Δk is imposed, which is responsible for Bloch oscillations in the frequency space. From the same dispersion relation, the highest group velocities in the frequency space are obtained for frequency momenta $k_f = \pm\pi/2$ and are directed in the positive and negative directions, respectively: the corresponding blue- and red-shifts of the input signal are reported in fig.2e,f, where we show the frequency dynamics of a light pulse injected with time delays $\Delta T = \pm\pi/2$ in a phase-matched ($\Delta k = 0$) system.

Dynamically Modulated Waveguide Arrays— While the previous results already give a hint of the potential of modulated waveguides as a tool to control the spectrum of broadband light pulses, we are now going to see how the modulation of CWAs can capitalize on topological photonics effects to increase the robustness of the spectral manipulation. To this purpose, let us now consider a 1D array of identical waveguides distributed along the x -direction separated by a constant distance d (fig.3a). For a sonic modulation propagating at an angle θ with respect to the waveguide axis, the dynamical modulation can be written in terms of the ℓ -th waveguide position $x_\ell = \ell d$ as $\Delta n_\ell(z, t) = 2b \cos(k_m^z z + k_m^x \ell d - \omega_m t)$, where $k_m^z = k_m \cos(\theta)$ and $k_m^x = k_m \sin(\theta)$ are, respectively, the longitudinal and orthogonal components of the modulation wavevector with respect to the waveguides axis. Analogous calculations with respect to the single waveguide case (see the Supplemental Materials [32] for details of the derivation) lead to the following set of propagation equations for the modal amplitude in the ℓ -th waveguide

at frequency ω

$$i\partial_z E_\ell(z, \omega) = \frac{\Delta k}{\omega_m} \omega E_\ell(z, \omega) - \beta e^{\pm i\ell\Phi} E_\ell(z, \omega \mp \omega_m) - \mathcal{B} E_{\ell\pm 1}(z, \omega) \quad (5)$$

where β is again the coupling coefficient in the frequency dimension, \mathcal{B} is the coupling coefficient in the spatial dimension which encapsulates the modal overlap between neighboring waveguides, Δk is the usual phase mismatch term and $\Phi = k_m d \sin(\theta)$.

For a narrowband incident pulse, it is again possible to discretize the frequency dimension by restricting to $\{\omega_n\} = \omega_0 + n\omega_m$. This leads to a 2D rectangular lattice (fig.3b) in a hybrid space composed by a spatial and a frequency dimension and to a propagation equation:

$$i\partial_z a_{\ell,n} = n \Delta k a_{\ell,n} - \beta e^{\pm i\ell\Phi} a_{n\mp 1, \ell} - \mathcal{B} a_{n, \ell\pm 1} \quad (6)$$

which takes the form of a Harper-Hofstadter (HH) model [24]. Because of the non-reciprocal phase term in the frequency-space coupling, proportional to β , a loop around a single plaquette of the rectangular lattice is in fact associated to a phase shift of $\Phi = \oint_C \mathbf{A} \cdot d\mathbf{r} = k_m d \sin(\theta)$. This phase shift is analogous to the geometric phase acquired by a charged particle in a constant magnetic field \mathbf{B} piercing the lattice.

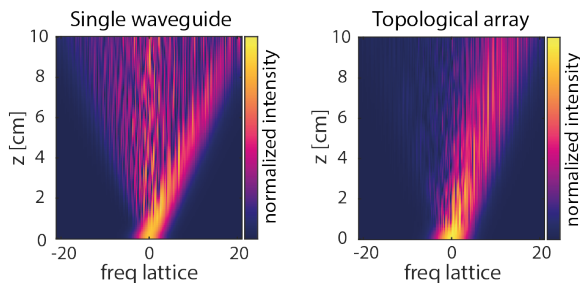


Fig. 4. Spectral power density distribution as a function of the propagation distance in the presence of a frequency-dependent refractive index disorder for a broadband beam propagating in a single modulated waveguide (left) or in a unidirectionally propagating edge mode of a topological array (right). Same parameters of Fig.2, the noise is uniformly distributed with maximum amplitude $\Delta n \approx \beta/k_0$

For a rational $\Phi = p/q$ (with p, q co-prime integers), the band-structure of the HH model is composed by q bands with non-trivial topological properties [24]. As a consequence of such non trivial topology, in a finite lattice geometry, chiral edge states appear within each bandgap. In particular, we consider a ribbon geometry with a finite extension along the spatial dimension and infinite in the frequency dimension. The resulting band-structure is shown in fig.3c: depending on the value of the frequency momentum k_f , mid-gap states appear with well defined and opposite group velocities, exponentially

localized at the opposite spatial edges of the waveguide array, indicated by the green and orange curves in the figure. Since only one state exist in each gap for each edge, they are immune to elastic back-scattering on disorder and allow for unidirectional transport, in our case along the frequency direction.

To demonstrate that unidirectional states with a specific chirality can be excited in a realistic experiment we inject a broadband input state with specific values of the frequency momenta k_f into the left-most waveguide of the array. As already described in the single waveguide case, the frequency momentum k_f corresponds to the time delay ΔT with respect to the dynamical modulation. Fig.3d shows how this procedure indeed results in the excitation of blue- or red-shifting topological modes, depending on the excited edge and frequency momenta: as one can see from the dispersion relation of the specific HH lattice under consideration, each edge supports indeed a single edge state for each value of k_f which avoids difficulties in selecting the desired propagation constant[33].

The key novelty of the topologically protected frequency transport in the hybrid frequency-space lattice is highlighted in fig.4. While in the clean system the frequency shift may look very similar to the one of the isolated waveguide configuration shown in figure 2(e,f), the behaviour in the presence of disorder is completely different. In the figure, we consider as an example a frequency-dependent refractive index, as it would be the case with an impure optical medium. For an isolated waveguide, such a disorder would induce a localization effect, so that the frequency conversion is inhibited (fig.4a). On the contrary, as shown in fig.4b, when happening through a topological mode the frequency shift is robust.

This result demonstrates the power of hybrid frequency-space lattices for shifting the carrier frequency of a broadband signal in a topologically protected way. In particular, the direction and the magnitude of the frequency shift can be controlled by the temporal delay ΔT of the incident pulse and the wavevector of the dynamical modulation. From the point of view of topological photonics, an exciting asset of our proposal consists in the possibility of varying the value of the synthetic magnetic field Φ through the properties of the sound wave and, in this way, span across models with different topological properties. Further manipulation tools are offered by the dispersion relation of the different waveguides [34] and/or the frequency-dependence of their refractive index [15, 32], which respectively induce external potentials along the spatial and frequency directions.

Conclusions and perspectives – In this work we have proposed a scheme to realize a hybrid frequency-space synthetic lattice subject to a synthetic magnetic field by acousto-optically modulating an array of waveguides. The strength of the synthetic field is controlled by the wavevector of the sound wave and, in turn, determines the topological properties of the lattice. The proposed

scheme paves the way to the use of the standard photonic technology of laser-written waveguides for the spectral manipulation of broadband signals. The coherent nature of the proposed scheme permits its application to classical waves (e.g. for time-to-frequency multiplexing conversion), as well as to single- or few-photon wavepackets, (e.g. to manipulate their entanglement between time, frequency and spatial variables), and opens the way to various applications in telecommunications and quantum science and technology.

ACKNOWLEDGEMENTS

FSP acknowledges fundings from Deutscher Akademischer Austauschdienst (grant n. 57507869). IC and FSP acknowledge financial support from the European Union H2020-FETFLAG-2018-2020 project “PhoQuS” (n.820392) and from the Provincia Autonoma di Trento, partly through the Q@TN initiative. AS acknowledges funding from the Deutsche Forschungsgemeinschaft (grants SCHE 612/6-1, SZ 276/12-1, BL 574/13-1, SZ 276/15-1, and SZ 276/20-1) and the Alfried Krupp von Bohlen and Halbach Foundation. FSP thanks Alberto Nardin for fruitful discussions.

* francesco.piccioli@unitn.it

- [1] S. Swaminathan and N. R. Raajan, Optical-orthogonal frequency division multiplexing-review, in *2017 IEEE International Conference on Power, Control, Signals and Instrumentation Engineering (ICPSI)* (2017) pp. 2644–2647.
- [2] A. Pe’Er, B. Dayan, A. A. Friesem, and Y. Silberberg, Temporal shaping of entangled photons, *Physical review letters* **94**, 073601 (2005).
- [3] T. Kobayashi, R. Ikuta, S. Yasui, S. Miki, T. Yamashita, H. Terai, T. Yamamoto, M. Koashi, and N. Imoto, Frequency-domain hong–ou–mandel interference, *Nature photonics* **10**, 441 (2016).
- [4] J. Roslund, R. M. De Araujo, S. Jiang, C. Fabre, and N. Treps, Wavelength-multiplexed quantum networks with ultrafast frequency combs, *Nature Photonics* **8**, 109 (2014).
- [5] H. Vural, S. L. Portalupi, and P. Michler, Perspective of self-assembled ingaas quantum-dots for multi-source quantum implementations, *Applied Physics Letters* **117**, 030501 (2020), <https://doi.org/10.1063/5.0010782>.
- [6] M. Colautti, F. S. Piccioli, Z. Ristanović, P. Lombardi, A. Moradi, S. Adhikari, I. Deperasinska, B. Kozankiewicz, M. Orrit, and C. Toninelli, Laser-induced frequency tuning of fourier-limited single-molecule emitters, *ACS Nano* **14**, 13584 (2020), pMID: 32936612, <https://doi.org/10.1021/acsnano.0c05620>.
- [7] H. Liu and A. S. Helmy, Joint measurement of time–frequency entanglement via sum frequency generation, *npj Quantum Information* **6**, 10.1038/s41534-020-00293-y (2020).
- [8] C. Q. Xu, H. Okayama, and M. Kawahara, 1.5 μm band efficient broadband wavelength conversion by difference frequency generation in a periodically domain-inverted linbo3 channel waveguide, *Applied Physics Letters* **63**, 3559 (1993), <https://doi.org/10.1063/1.110096>.
- [9] H. Takesue, Erasing distinguishability using quantum frequency up-conversion, *Phys. Rev. Lett.* **101**, 173901 (2008).
- [10] B. A. Bell, K. Wang, A. S. Solntsev, D. N. Neshev, A. A. Sukhorukov, and B. J. Eggleton, Spectral photonic lattices with complex long-range coupling, *Optica* **4**, 1433 (2017).
- [11] J. H. Weber, B. Kambs, J. Kettler, S. Kern, J. Maisch, H. Vural, M. Jetter, S. L. Portalupi, C. Becher, and P. Michler, Two-photon interference in the telecom c-band after frequency conversion of photons from remote quantum emitters, *Nature Nanotechnology* **14**, 23 (2019).
- [12] W. Li, C. Qin, T. Han, H. Chen, B. Wang, and P. Lu, Bloch oscillations in photonic spectral lattices through phase-mismatched four-wave mixing., *Optics letters* **44**, 5430 (2019).
- [13] Z. Gaburro, M. Ghulinyan, F. Riboli, L. Pavesi, A. Recati, and I. Carusotto, Photon energy lifter, *Opt. Express* **14**, 7270 (2006).
- [14] S. F. Preble, Q. Xu, and M. Lipson, Changing the colour of light in a silicon resonator, *Nature Photonics* **1**, 293 (2007).
- [15] T. Ozawa, H. M. Price, N. Goldman, O. Zilberberg, and I. Carusotto, Synthetic dimensions in integrated photonics: From optical isolation to four-dimensional quantum hall physics, *Phys. Rev. A* **93**, 043827 (2016).
- [16] L. Yuan, Y. Shi, and S. Fan, Photonic gauge potential in a system with a synthetic frequency dimension, *Opt. Lett.* **41**, 741 (2016).
- [17] L. Yuan, Q. Lin, M. Xiao, and S. Fan, Synthetic dimension in photonics, *Optica* **5**, 1396 (2018).
- [18] L. Yuan, A. Dutt, and S. Fan, Synthetic frequency dimensions in dynamically modulated ring resonators, *APL Photonics* **6**, 071102 (2021).
- [19] S. Buddhiraju, A. Dutt, M. Minkov, and S. Fan, Arbitrary linear transformations for photons in the frequency synthetic dimension, *Nature Communications* **12**, 2401 (2021).
- [20] C. Qin, L. Yuan, B. Wang, S. Fan, and P. Lu, Effective electric-field force for a photon in a synthetic frequency lattice created in a waveguide modulator, *Phys. Rev. A* **97**, 063838 (2018).
- [21] C. Qin, F. Zhou, Y. Peng, D. Sounas, X. Zhu, B. Wang, J. Dong, X. Zhang, A. Alù, and P. Lu, Spectrum control through discrete frequency diffraction in the presence of photonic gauge potentials, *Phys. Rev. Lett.* **120**, 133901 (2018).
- [22] C. Qin, B. Wang, Z. J. Wong, S. Longhi, and P. Lu, Discrete diffraction and bloch oscillations in non-hermitian frequency lattices induced by complex photonic gauge fields, *Phys. Rev. B* **101**, 064303 (2020).
- [23] C. Qin, Q. Liu, B. Wang, and P. Lu, Photonic weyl phase transition in dynamically modulated brick-wall waveguide arrays, *Opt. Express* **26**, 20929 (2018).
- [24] T. Ozawa, H. M. Price, A. Amo, N. Goldman, M. Hafezi, L. Lu, M. C. Rechtsman, D. Schuster, J. Simon, O. Zilberberg, and I. Carusotto, Topological photonics, *Rev. Mod. Phys.* **91**, 015006 (2019).

- [25] D. Leykam and L. Yuan, Topological phases in ring resonators: recent progress and future prospects, *Nanophotonics* **9**, 4473 (2020).
- [26] L. Yuan, M. Xiao, Q. Lin, and S. Fan, Synthetic space with arbitrary dimensions in a few rings undergoing dynamic modulation, *Phys. Rev. B* **97**, 104105 (2018).
- [27] E. Lustig, S. Weimann, Y. Plotnik, Y. Lumer, M. A. Bandres, A. Szameit, and M. Segev, Photonic topological insulator in synthetic dimensions, *Nature* **567**, 356 (2019).
- [28] L. Nemirovsky, M.-I. Cohen, Y. Lumer, E. Lustig, and M. Segev, Synthetic-space photonic topological insulators utilizing dynamically invariant structure, *Phys. Rev. Lett.* **127**, 093901 (2021).
- [29] T. Ozawa, Artificial magnetic field for synthetic quantum matter without dynamical modulation, *Phys. Rev. A* **103**, 033318 (2021).
- [30] A. Dutt, Q. Lin, L. Yuan, M. Minkov, M. Xiao, and S. Fan, A single photonic cavity with two independent physical synthetic dimensions, *Science* **367**, 59 (2020).
- [31] A. Szameit and S. Nolte, Discrete optics in femtosecond-laser-written photonic structures, *Journal of Physics B: Atomic, Molecular and Optical Physics* **43**, 163001 (2010).
- [32] Supporting Informations available online.
- [33] S. Stützer, Y. Plotnik, Y. Lumer, P. Titum, N. H. Lindner, M. Segev, M. C. Rechtsman, and A. Szameit, Photonic topological anderson insulators, *Nature* **560**, 461 (2018).
- [34] C. Oliver, I. Carusotto, and H. M. Price, to be submitted (2021).

Topologically protected frequency control of broadband signals in dynamically modulated waveguide arrays

Supplementary Informations

Francesco S. Piccioli,^{1,2} Alexander Szameit,² and Iacopo Carusotto^{1,3}

¹University of Trento and CNR-INO BEC center, Via Sommarive 14, 38123 Povo (TN), Italy

²Institute for Physics, University of Rostock, Albert-Einstein-Str. 23, 18059 Rostock, Germany

³Corresponding author: iacopo.carusotto@unitn.it

DERIVATION OF THE EQUATION OF MOTION FOR A SINGLE MODULATED WAVEGUIDE

Let's consider paraxial light propagation in an optical waveguide with the axis aligned to the z -direction. Under the assumption of slowly varying refractive index modulation, the modal amplitude of the electric field is also assumed to vary slowly, and the paraxial Helmholtz equation can be rewritten as a schroedinger-like equation

$$i\partial_z \mathcal{E}(z, t) = -k\mathcal{E}(z, t) - \Delta n k_0 \mathcal{E}(z, t) \quad (1)$$

Here k is the light wavevector that is a function of the temporal derivative and the dispersion. We consider a refractive index perturbation that has a travelling monochromatic wave profile such as

$$\Delta n(r, t) = 2\delta n \cos(\mathbf{k}_m \cdot \mathbf{r} - \omega_m t) \quad (2)$$

Since the typical optical waveguide width is much smaller than the wavelength of the perturbation, we assume the perturbation phase to be constant in the transverse plane therefore we can rewrite the modulation as

$$\Delta n(z, t) 2\delta n \cos(k_m^z z - \omega_m t) \quad (3)$$

where $k_m^z = k_m \cos(\theta)$, being θ the angle of the modulation wave with respect to the waveguide axis, is the z -component of the modulation wavevector. We move to the frequency space and rewrite (1) as

$$i\partial_z \mathcal{E}(z, \omega) = -\kappa_l(\omega) \mathcal{E}(z, \omega) - k_0 \Delta n(z, \omega) \circledast \mathcal{E}(z, \omega) \quad (4)$$

Where \circledast denotes convolution in the frequency space, $\Delta n(z, \omega) = \delta n e^{\pm i k_m^z z} \delta(\omega \mp \omega_m)$ is the Fourier Transform of $\Delta n(z, t)$ and $k(\omega)$ is the light wavevector that we can expand around ω_0 as $k(\omega) = k_0 + \frac{\omega - \omega_0}{v_g}$, being v_g the group velocity in the waveguiding structure. We now perform a gauge transformation and move to the light wave reference frame by defining

$$\mathcal{E}(z, \omega) = \tilde{\mathcal{E}}(z, \omega) e^{i k(\omega) z} \quad (5)$$

with this substitution the equation for $\tilde{\mathcal{E}}(z, \omega)$ reads

$$i\partial_z \tilde{\mathcal{E}}(z, \omega) = -k_0 \delta n e^{\pm i (k_m - \frac{\omega_m}{v_g}) z} \tilde{\mathcal{E}}(z, \omega \mp \omega_m) \quad (6)$$

In which we used the fact that $k(\omega \pm \omega_m) - k(\omega) = \pm \frac{\omega_m}{v_g}$. We define the phase mismatch between the light wave and the perturbation as $\Delta k = k_m - \frac{\omega_m}{v_g}$ and perform another gauge transformation

$$\tilde{\mathcal{E}}(z, \omega) = E e^{i \frac{\omega}{\omega_m} \Delta k z} \quad (7)$$

which allows to write the equation for E :

$$i\partial_z E = \frac{\Delta k}{\omega_m} \omega E - \beta E(\omega \mp \omega_m) \quad (8)$$

Where $\beta = k_0 \delta n$ is a coupling coefficient. The diagonal term $\frac{\Delta k}{\omega_m} \omega E(z, \omega) = V \omega E(z, \omega)$ plays the role of an on-site energy increasing in the direction of increasing frequencies, which is the analogue of a constant scalar potential. The scalar potential V is proportional to the phase mismatch:

$$V \propto \Delta k = k_m^z - \omega_m \frac{\partial k}{\partial \omega} = k_m \cos \theta - \frac{\omega_m}{v_g} \quad (9)$$

Where $v_g \approx c_0/n$ is the group velocity of light in the waveguide. Satisfying the phase matching condition means $\Delta k = 0$ in (9). As the light wavevector is extremely small, one can typically assume $\Delta k \approx k_m \cos \theta$. However $k_m = \frac{2\pi\omega_m}{c_m}$, where c_m is the speed of the modulation wave is a significant quantity. As a result the slightest deviation from the optimal propagation angle $\theta = \pm\pi/2$ makes the phase mismatch too strong to observe any dynamics in the synthetic space at all. As we further discuss in the implementation section this motivates the need of precisely controlling the direction of the light wave which is a notable experimental effort.

DERIVATION OF THE EQUATION OF MOTION FOR A MODULATED WAVEGUIDE ARRAY

Let's now consider a modulated waveguide array. If we consider no coupling between the individual waveguides then each waveguide of the array can be described by an equation analogous to (1). On the other side, if the waveguides are weakly coupled (1) is modified to include a coupling coefficient between the waveguides yielding the following set of equations for the ℓ -th waveguide of an array

$$i\partial_z \mathcal{E}_\ell(z, t)_\ell = -k\mathcal{E}_\ell - k_0\Delta n(z, t)\mathcal{E}_\ell(z, t) - k_0J\mathcal{E}(z, t)_{\ell\pm 1} \quad (10)$$

Where we assumed the waveguides to be all identical such that $k_\ell = k$.

The refractive index perturbation, as previously considered, is a travelling wave described by

$$\Delta n(z, t) = 2\delta n \cos(\mathbf{k}_m \cdot \mathbf{r} - \omega_m t) \quad (11)$$

We consider the waveguides to be evenly distributed along the x -direction with an inter-waveguide distance d that we assume to be much larger than the waveguide width. The phase of the perturbation is therefore different in each individual waveguide, but can be considered constant across the width of each waveguide. To this aim we discretize the space in the x -direction and define the position of the ℓ -th waveguide as $x_\ell = d\ell$. The refractive index perturbation can be rewritten as

$$\Delta n_\ell(z, t) = 2\delta n \cos(k_m^z z + k_m^x d\ell - \omega_m t) \quad (12)$$

where $k_m^z = k_m \cos(\theta)$ is the longitudinal component while $k_m^x = k_m \sin(\theta)$ is the transverse component of the modulation wavevector. Following the same steps of the single waveguide case we move to the frequency space and rewrite (10) as

$$i\partial_z \mathcal{E}_\ell(z, \omega) = -k(\omega)\mathcal{E}_\ell(z, \omega) - k_0\Delta n_\ell(z, \omega)\mathcal{E}_\ell(z, \omega) - k_0J\mathcal{E}_{\ell\pm 1}(z, \omega) \quad (13)$$

In this case $\Delta n(z, \omega)$ is the Fourier transform of $\Delta n(z, t)$ and is written as $\Delta n_\ell(z, \omega) = e^{\pm i(k_m^z z + k_m^x \ell d)}\delta(\omega \mp \omega_m)$. We apply to each waveguide the gauge transformation defined in (5) and rewrite (10) as:

$$i\partial_z \tilde{\mathcal{E}}_\ell(z, \omega) = -\beta e^{\pm i\Delta k z} e^{\pm \Phi \ell} \tilde{\mathcal{E}}_\ell(z, \omega \mp \omega_m) - \mathcal{B} \tilde{\mathcal{E}}_{\ell\pm 1}(z, \omega) \quad (14)$$

Where $\Delta k = k_m \cos \theta - \frac{\omega_m}{v_g}$ is the usual phase mismatch term, $\Phi = dk_m \sin \theta$ is the modulation phase difference between two closest waveguides, β is the coupling coefficient in the frequency space and \mathcal{B} is the coupling coefficient in the physical space. Using once again (7) on each waveguide we can rewrite the latter as

$$i\partial_z E_\ell(z, \omega) = V\omega E_\ell(z, \omega) - \beta e^{\pm \Phi \ell} E_\ell(z, \omega \mp \omega_m) - \mathcal{B} E_{\ell\pm 1}(z, \omega) \quad (15)$$

SUPPORTING INFORMATIONS

Discretization of the equation and numerical methods

Equations (8) and (15) are written considering the light frequency as a continuous dimension. The dynamical modulation induces long range hoppings in such a continuous dimension between frequencies spaced by multiples of ω_m . Therefore if one considers a monochromatic input beam at ω_0 the symmetry allows to restrict the frequencies of interest to a discrete set $\{\omega_n\} = \omega_0 + n\omega_m$ with $n \in \mathbb{Z}$. With this assumption we define $E_\ell(z, \omega_0 + n\omega_m) = a_{n,\ell}(z)$ and rewrite (8),(15) as

$$i\partial_z \tilde{a}_n(z) = (q_0 + n\Delta k)\tilde{a}_n(z) - \beta \tilde{a}_{n\mp 1}(z) \quad (16)$$

$$i\partial_z \tilde{a}_{n,\ell}(z) = (q_0 + n\Delta k)\tilde{a}_{n,\ell}(z) - \beta e^{\pm \Phi \ell} \tilde{a}_{n\mp 1,\ell}(z) - \mathcal{B} \tilde{a}_{n,\ell\pm 1}(z) \quad (17)$$

After which the constant wavevector q_0 can be removed by the gauge transformation $\tilde{a}_{n,\ell}(z) = a_{n,\ell}(z)e^{iq_0z}$. The fully discretized equations (16) and (17) can be translated into a set of $N \times L$ differential equations, where L is the dimension of the physical space (i.e. the number of waveguides in the array) and N is the dimension of the frequency space (i.e. the number of considered frequencies) that can be solved using MATLAB's numerical tools. In the main text we consider broadband gaussian input beams with different bandwidths. To model the behaviour of a broadband pulse we discretize the frequency space in $N \times h$ frequency bins in such a way that a frequency interval ω_m gets divided into h identical segments $\delta\omega = \frac{\omega_m}{h}$. (16) and (17) translate into a set $N \times h \times L$ of differential equations that are solved using MATLAB's numerical tools.

Edge Effects in Frequency space

Whereas the truncation of the waveguide array constitutes a fundamental bound to the physical dimension, the frequency dimension is unbounded. A parabolic confining potential arises in the presence of group velocity dispersion (i.e. $\frac{\partial^2 k_l}{\partial \omega^2} \neq 0$) however this typically kicks in when sizable frequency shifts are considered which is not the case in our model. A detailed discussion of this higher order effect will be the subject of a future work.

In order to neglect artificial edge effects in the numerical calculations presented in the main text, we always consider a frequency extension of the system that is bigger than the maximum achievable frequency shift for a given propagation distance z_{\max} .

However edge effects can be also be interesting. To inspect the effect of hard edges on the propagation in the synthetic dimension we consider a strong absorption at a specific frequency ω_a , which acts as an impenetrable wall in the frequency space. If the absorption spectrum $\Delta\omega_a > \omega_m$ all the frequency components of an impinging wavepacket will likewise experience the hard edge. As a result, the wavepacket will be deflected with perfect transmission around the corner of the hybrid space (see fig. 1 left). If the absorption spectrum is narrowband the behaviour is qualitatively different. While propagating along the synthetic dimension, frequency bins corresponding to $\Delta\omega_a$ are chopped from the wavepacked and deflected along the physical dimension with perfect transmission. The remaining wavepacket, keeps propagating along the frequency dimension in the form of an up-shifting frequency comb (see fig 1 right)

NOTES ON EXPERIMENTAL IMPLEMENTATION

Our model takes advantage of the continuous spectrum of modes in waveguides and allows to effectively manipulate a TLC signal with arbitrary frequency spectrum. Previous works have been focused on the modulation of isolated LiNbO₃ waveguides using microwaves and the electro optical effect [1, 2]. However LiNbO₃ waveguides require complex fabrication procedure and the technology is not suited for the realization of coupled waveguide arrays, as the strong confinement of the light field makes the evanescent coupling negligible. Furthermore, refractive index variation via RF modulation requires a strong electro-optical coefficient which is available in few materials and especially not in amorphous ones, that are more suited for the realization of coupled waveguides arrays [3]

As a different paradigm we propose the use of acoustic waves to perform dynamical modulation of optical waveguide arrays fabricated using femtosecond laser writing in SiO₂ glass [3].

The numerical calculations presented in the main text assume a modest refractive index increase of $2 \cdot 10^{-5}$ that, using a 100 MHz acoustic wave generates frequency shift of ≈ 800 MHz after a 10 cm propagation into a single modulated waveguide. Higher frequency shifts are achievable using higher frequency acoustic waves, up to the point where higher order phenomena becomes important such as the dispersion of the coupling coefficient in the frequency space or the parabolic confining potential in the frequency space caused by group velocity dispersion. However the higher the frequency of the dynamical modulation the more dramatic is the effect of phase mismatch, thus a mechanism to enforce directional excitation of the sound wave with high precision is required. To this aim, we suggest to excite the sound wave using an array of emitters. On one hand multiple emitters allow to shape the front of the acoustic wave, thus getting closer to the ideal plane wave front. On the other hand, the use of multiple equi-spaced emitters with an externally controllable phase relation allows to effectively control the propagation angle of the modulation. The ability to electronically control the phase relation between different emitters would also allow the realization of reconfigurable devices.

Previous works have inspected the propagation of pressure waves in bulk fused silica samples [4] characterizing the acousto-optical effect on ion-diffused waveguide structures in a low acoustic-frequency regime. Despite the attractiveness of bulk acoustic waves, that would allow to perform dynamical modulation of two dimensional waveguide arrays

hence potentially achieving an effective 3D physics [5], the power decay of spherical waves is too fast to allow for an homogeneous modulation of large waveguide arrays.

To overcome this issue, in the recent years, a strong effort has been devoted to the integration of Surface Acoustic Waves (SAW) technologies [6]. Being confined to the surface, the power scaling with the travelled distance is in fact much slower, allowing to conserve the acoustic power throughout the entire sample length. Moreover, SAW transducers can be realized with extremely high operating frequencies [6, 7], leading to bigger frequency shifts in our proposed modulator.

SAW are typically excited using InterDigitalized Transducer (IDTs), whose fabrication is compatible with standard lithographic process and is particularly suited for the realization of emitter arrays[6]. In particular, in our proposed scheme, IDTs arrays could be lithographed on the fused silica glass after sputtering the surface of the sample with a piezoelectric film as in figure 2. Although in this scheme the SAW is peaked in the thin piezoelectric layer, if the optical waveguides are realized sufficiently close to the interface a reasonable overlap is expected [7] between the evanescent tail of the acoustic wave (in the order of an acoustic wavelength) and the optical mode field, leading to the required effective index modulation.

-
- [1] C. Qin, L. Yuan, B. Wang, S. Fan, and P. Lu, Effective electric-field force for a photon in a synthetic frequency lattice created in a waveguide modulator, *Phys. Rev. A* **97**, 063838 (2018).
 - [2] C. Qin, B. Wang, Z. J. Wong, S. Longhi, and P. Lu, Discrete diffraction and bloch oscillations in non-hermitian frequency lattices induced by complex photonic gauge fields, *Phys. Rev. B* **101**, 064303 (2020).
 - [3] A. Szameit and S. Nolte, Discrete optics in femtosecond-laser-written photonic structures, *Journal of Physics B: Atomic, Molecular and Optical Physics* **43**, 163001 (2010).
 - [4] L. Poffo, P. Lemaître-Auger, P. Benech, and P. Benech, Determination of refractive index variation of a glass-integrated optical waveguide by the acousto-optic effect, *Measurement Science and Technology* **20**, 045303 (2009).
 - [5] C. Qin, Q. Liu, B. Wang, and P. Lu, Photonic weyl phase transition in dynamically modulated brick-wall waveguide arrays, *Opt. Express* **26**, 20929 (2018).
 - [6] P. Delsing, A. N. Cleland, M. J. A. Schuetz, J. Knörzer, G. Giedke, J. I. Cirac, K. Srinivasan, M. Wu, K. C. Balram, C. Bäuerle, T. Meunier, C. J. B. Ford, P. V. Santos, E. Cerda-Méndez, H. Wang, H. J. Krenner, E. D. S. Nysten, M. Weiß, G. R. Nash, L. Thevenard, C. Gourdon, P. Rovillain, M. Marangolo, J.-Y. Duquesne, G. Fischerauer, W. Ruile, A. Reiner, B. Paschke, D. Denysenko, D. Volkmer, A. Wixforth, H. Bruus, M. Wiklund, J. Reboud, J. M. Cooper, Y. Fu, M. S. Brugger, F. Rehfeldt, and C. Westerhausen, The 2019 surface acoustic waves roadmap, *Journal of Physics D: Applied Physics* **52**, 353001 (2019).
 - [7] S. A. Tadesse and M. Li, Sub-optical wavelength acoustic wave modulation of integrated photonic resonators at microwave frequencies, *Nature Communications* , 5402 (2014).

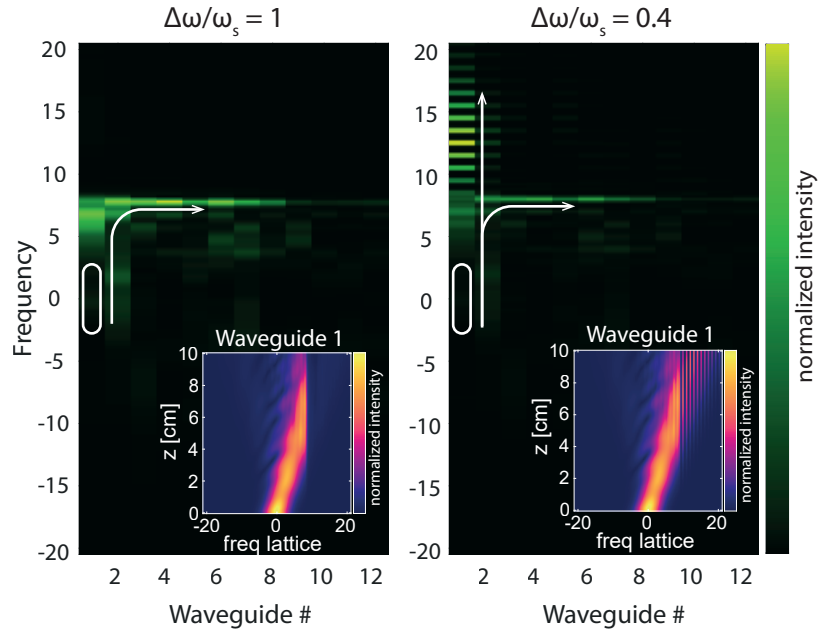


Fig. 1. Spectral power density distribution in each waveguide after a propagation of 10 cm when a strong absorption, centered at $\frac{\omega}{\omega_s} = 9$, is considered. **left:** Broadband absorption acts as an effective hard-wall for the whole wavepacket. **right:** Narrowband absorption acts as an effective hard wall for a fraction of the wavepacket, while the remaining part propagates unaffected. **inset:** spectral power density distribution as a function of the propagation distance in the leftmost waveguide of the array.

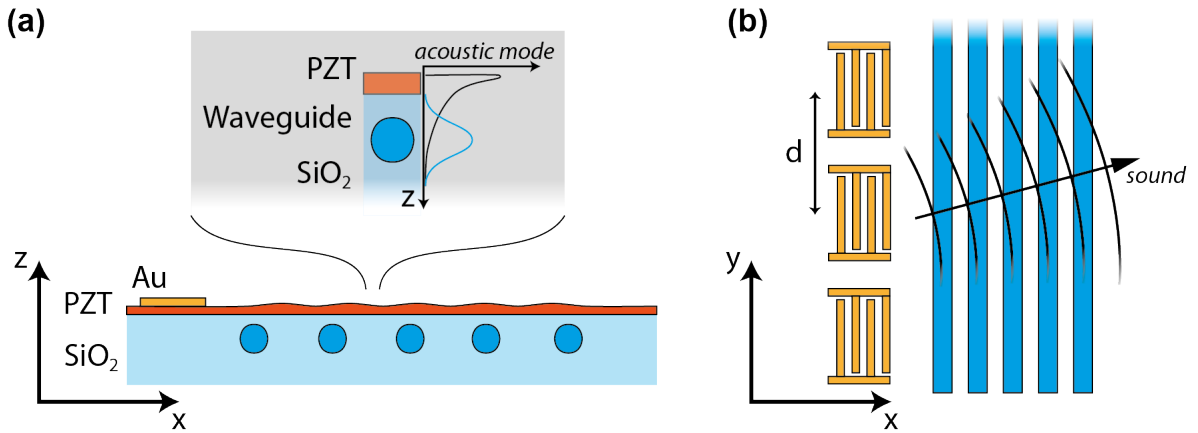


Fig. 2. Schematic of the proposed experiment. **(a):** Front view of the device. A thin layer of a piezoelectric material is deposited on a SiO₂ sample with surface waveguides. inset: The evanescent tail of the Rayleigh wave supported by the Piezo layer leaks into the fused silica waveguide modulating the refractive index via the acousto-optic effect. **(b):** Top view of the device. InterDigitalized Transducers (IDTs) with a fixed distance d are lithographed on the sample surface.